

Automatic deformable registration of histological slides to μ CT volume data

N. Chicherova^{*,†}, S.E. Hieber[†] , A. Khimchenko[†], C. Bikis[†], B. Müller[†] & P. Cattin^{*}

^{*}Center for medical Image Analysis & Navigation, Department of Biomedical Engineering, University of Basel, Allschwil, Switzerland

[†]Biomaterials Science Center, Department of Biomedical Engineering, University of Basel, Allschwil, Switzerland

Key words. 2D-3D registration, histology, micro computed tomography, multimodal, slice-to-volume registration.

Summary

Localizing a histological section in the three-dimensional dataset of a different imaging modality is a challenging 2D-3D registration problem. In the literature, several approaches have been proposed to solve this problem; however, they cannot be considered as fully automatic. Recently, we developed an automatic algorithm that could successfully find the position of a histological section in a micro computed tomography (μ CT) volume. For the majority of the datasets, the result of localization corresponded to the manual results. However, for some datasets, the matching μ CT slice was off the ground-truth position. Furthermore, elastic distortions, due to histological preparation, could not be accounted for in this framework.

In the current study, we introduce two optimization frameworks based on normalized mutual information, which enabled us to accurately register histology slides to volume data. The rigid approach allocated 81 % of histological sections with a median position error of 8.4 μ m in jaw bone datasets, and the deformable approach improved registration by 33 μ m with respect to the median distance error for four histological slides in the cerebellum dataset.

Introduction

Histology slides generally form the basis of a quantitative analysis of tissue morphology. Because the two-dimensional slide represents only a part of the three-dimensional object, the conclusions may depend on the slide selection, see, e.g. (Bernhardt *et al.*, 2004). Micro computed tomography (μ CT) yields the full three-dimensional information in a nondestructive fashion and is, therefore, complementary to the histological analysis. If the morphological information is at least partially available in both data, one can extrapolate the information

from histology to the third dimension (Hieber *et al.*, 2016; Khimchenko *et al.*, 2016). Furthermore, it is well known that the preparation of histology slides gives rise to artefacts, including cracks and location-dependent shrinkage (Germann *et al.*, 2008; Schulz *et al.*, 2011). Using even less detailed CT data, one can correct the slides to obtain more reliable results. For the artefact correction, the selection of an optimized cutting direction and the extrapolation into the third dimension, a sound identification of the two-dimensional counterpart of the histological slide in the three-dimensional tomography dataset is necessary. Image registration is the basis for numerous image analysis techniques. In particular, the registration of images from different modalities enables practitioners to obtain a large amount of complementary information for accurate diagnosis (Zhan *et al.*, 2007; Alic *et al.*, 2011; Seise *et al.*, 2011; Goubran *et al.*, 2015), the combination of functional and morphological data (Schormann & Zilles, 1998; Müller *et al.*, 2012; Particelli *et al.*, 2012; Schulz *et al.*, 2012; Stalder *et al.*, 2014) or atlas construction (Ourselin *et al.*, 2001; Tsai *et al.*, 2008; Krauth *et al.*, 2010; Tsai *et al.*, 2011), to name but a few. The task is particularly challenging when aligning multimodal data of different dimensions, such as 2D to 3D. There exist many techniques for 2D projections to 3D volume registration (Markelj *et al.*, 2012). None of them can be applied to our problem, i.e. matching a histological slide to a tomographic volume dataset acquired from the same specimen, because of two main reasons. First, the basic goal of these algorithms is to find a mapping between the projections and the 3D volume. Second, the methods often require manual feature identification. In contrast, our 2D-3D registration problem is concerned with registering a 2D slide such as histological section to a 3D dataset, i.e. slice-to-volume registration. In the literature, it is commonly referred to as slice-to-volume registration (Ferrante & Paragios, 2017) and only a few approaches investigate the problem of registering 2D histology images to 3D datasets as well as 2D-2D multimodal registration of histological images (Jacobs *et al.*, 1999; du Bois d'Aische *et al.*, 2005; Li *et al.*, 2006; Pitiot *et al.*, 2006).

Correspondence to: Simone E. Hieber, Biomaterials Science Center, Department of Biomedical Engineering, University of Basel, Allschwil 4123, Switzerland. Tel: +41 61 207 54 33; fax: +41 61 207 54 99; e-mail: simone.hieber@unibas.ch

The most common approaches for registering histological sections to the 3D space initially reconstruct a 3D volume from histology serial sections and then apply 3D-3D registration (Ourselin *et al.*, 2001; Ceritoglu *et al.*, 2010; Alic *et al.*, 2011; Nir & Salcudean, 2013). Reconstructing a 3D volume from 2D histological sections, however, requires information about the sectioning location in 3D space, which is not always available. One way of determining this information is to use a complementary modality such as blockface photographs (Kim *et al.*, 1997; Schormann & Zilles, 1998; Meyer *et al.*, 2006; Dauguet *et al.*, 2007; Park *et al.*, 2008; Liu *et al.*, 2012; Goubran *et al.*, 2013; Hallack *et al.*, 2015) or photographs of an unstained brain (Bardinet *et al.*, 2002). Hallack *et al.* (2015) performed a three-stage procedure for the registration of a histology stack to an *ex-vivo* MRI dataset using feature points: (1) Matching image stack to MRI dataset, (2) rigid registration of each histological slide to MRI slice (3) and nonrigid registration. Some of the methods rely on implanting artificial markers (Humm *et al.*, 2003; Lazebnik *et al.*, 2003; Breen *et al.*, 2005) or color-coding (Alic *et al.*, 2011). Many reconstruction strategies utilize segmentation (Taylor *et al.*, 2004; Zhan *et al.*, 2007; Ou *et al.*, 2009) for volume reconstruction or for more robust similarity calculations (Ourselin *et al.*, 2001; Mosaliganti *et al.*, 2006; Seise *et al.*, 2011; Nir & Salcudean, 2013). There are also 3D reconstruction techniques based on mutual similarities between 2D histological images and known or fixed spacing between slides (Ourselin *et al.*, 2001; Arganda-Carreras *et al.*, 2010; Nir & Salcudean, 2013). The main limitation of these 3D-3D registration techniques is that they require a high number of histological sections that are not always available.

Our approach differs from the one of Hallack *et al.* (2015) in the respect that one single slide can be registered directly to the 3D dataset and that the matching surface can be curved to adapt to large deformations. In our work, we focus on a more challenging type of histology registration, namely single slide-to-volume registration (Sarve *et al.*, 2008). One of the most recent approaches by Hoerth *et al.* (2015) registered semiautomatically 2D images within 3D μ CT data, using the generalized Hough transform. Lundin *et al.* (2017) presented an accurate approach based on binary data that requires a presegmentation step and is tailored to trabecular bone. In Wachowiak *et al.* (2004), the authors applied a global optimization for rigid 2D CT and simulated ultrasound slices (USs) to 3D histology registration. With normalized mutual information (NMI) as a cost function, the optimal parameters for particle swarm optimization were determined. Ferrante & Paragios (2013) based the registration on a grid of control points that represents both in- and out-of-plane deformation. By pairwise over-parametrization of the graphical model, they overcome inefficiency of the proposed model. The real-time registration of US slices to MRI explored by Pardasani *et al.* (2016) was able to improve the initial pose using patch-based similarity. Several methods also account for nonlinear deformations perpendicular to the slicing plane, which can often occur

in soft tissue specimens (Schormann *et al.*, 1995; Kim *et al.*, 2000; Dauguet *et al.*, 2007; Goubran *et al.*, 2015). Among nonrigid registration techniques applied to histology, one can find methods based on splines (Dauguet *et al.*, 2007; Osechinskiy & Kruggel, 2010) or on a radial basis (Goubran *et al.*, 2015) which require a selection of control points and a full multigrid approach (Schormann & Zilles, 1998). One of the attempts to incorporate nonrigid deformation was made by Osechinskiy & Kruggel (2010), who introduced a general framework for slice deformation in 3D space and implemented different techniques to identify the best-performing set of parameters. Slide-to-volume registration was also investigated by Kim *et al.* (2000), who used nonlinear polynomial functions to relate the coordinates of 2D histology to 3D MRI. Although these methods achieve reasonable results in registration, they need manual interventions at the stage of either segmentation or near ground truth initialization, where the ground truth corresponds to the best fit.

Manual detection of the histological slide in a 3D volume is a very time-consuming task and can last up to 1 day for one slide. Recently, we have developed an automatic algorithm for 2D histology to 3D μ CT localization (Chicherova *et al.*, 2014) and showed its application on jaw bone data. Although the algorithm performed very well for most of the specimens, in some cases localization improvement was needed. In this paper, we extend the framework by registering more accurately each histological slide into the volume. We propose a combined rigid and deformable registration approach for hard and soft tissue samples. The main elements of the proposed method are NMI (Viola & Wells III, 1997; Studholme *et al.*, 1999; Pluim *et al.*, 2003) and Legendre polynomials, which are used as basis functions to approximate surface deformation. In addition to being fully automatic, the proposed method is significantly more accurate than the first approach introduced by Chicherova *et al.* (2014).

Materials and methods

We used two datasets to evaluate the performance of the two-step optimization frameworks. The first dataset originated from a dental study about jaw bone augmentation materials (Stalder *et al.*, 2014). The bone specimens were extracted from patients directly before inserting the dental implants. The procedure was approved by the responsible Ethical Committee, study protocol number 290/13, to perform a combined histology and tomography study. Five male and four female patients, aged between 46 and 75 years, obtained treatments of bone defects at the molars in the upper and lower jaw ($n = 8$ and $n = 1$, respectively). The bone graft materials used were BoneCeramic[®] (Institute Straumann AG, Basel, Switzerland) in one case, easy-graftTM (SUNSTAR Degradable Solutions AG, Schlieren, Switzerland) in four cases and Bio-Oss[®] (Geistlich Biomaterials, Wolhusen,

Table 1. List of tomograms including specimen specifications.

#	Patient	age (Gender) [years]	Biopsy location ISO 3950	Grafting material	Dataset voxel length [μm]	Dataset size [voxel]	No. of slides
1	A	70(m)	11	easy-graft TM	4.3	861×861×1939	6
2	B	74(f)	11	easy-graft TM	8.6	301×301×969	9
3	C	46(m)	23	Bio-Oss [®]	8.6	301×301×1093	7
4	D	47(m)	16	BoneCeramic [®]	8.6	421×421×753	6
5	E	57(m)	34	easy-graft TM	8.6	301×301×507	6
6	F	75(m)	16	Bio-Oss [®]	8.6	320×320×718	4
7	G	63(f)	15	BoneCeramic [®]	8.6	440×440×738	5
8	H	46(f)	21	easy-graft TM	8.6	300×300×799	6
9	I	47(f)	26	Bio-Oss [®]	8.6	381×381×416	4
10	E	57(m)	34	easy-graft TM	4.3	621×621×1269	5

Datasets #9 and #10 were not considered in the standard error analysis because they required an adjustment of the setup (see Section 3.1) for a successful registration.

Switzerland) in three cases (Table 1). After 5 months, the biopsy was harvested with a trephine bur 3 mm in diameter exactly at the position for implant placement. These biopsies were composed of soft tissues, existing and newly formed bone, as well as augmentation and embedding materials (Stalder *et al.*, 2014). The pathology samples were cylindrical biopsies with a diameter of around 2 mm and a length of approximately 4 mm. In order to analyze the integration of the graft in the jaw, a μCT of the whole specimen was acquired. The jaw biopsies were scanned using synchrotron radiation-based micro computed tomography (SR μCT). The measurements were performed at the beamline W2 (HASY-LAB/DESY, Hamburg, Germany, operated by HZG Research Center, Geesthacht, Germany) in conventional absorption contrast mode. The photon energy corresponded to 25 keV. The detector featured 3056×3056 pixels (effective pixel length $2.2 \mu\text{m}$), which were binned by a factor of two before reconstruction to increase the density resolution (Thurner *et al.*, 2004). The tomogram was obtained from a set of 721 equiangular radiographs along 180° using the standard filtered back-projection reconstruction algorithm (Stalder *et al.*, 2014). The cerebellum specimen was scanned using the CT-system nanotom[®] m (phoenix | X-ray, GE Sensing & Inspection Technologies GmbH, Wunstorf, Germany) in absorption contrast mode with an accelerating voltage of 60 kV and a voxel length of $3.5 \mu\text{m}$. The dataset was resized to a voxel length of $7 \mu\text{m}$ using MATLAB[®] R2016a (The MathWorks, 135 Inc., Natick, MA, U.S.A.). Subsequently, five to nine histological cross-sections through the horizontal plane of the specimen were taken. After the SR μCT data acquisition, the biopsies were placed in customized polytetrafluoroethylene molds and embedded with a methyl methacrylate solution consisting of methacrylate-methyl ester (Sigma-Aldrich Chemie GmbH, Buchs, Switzerland); dibutyl phthalate (Merck-Schuchardt OHG, Hohenbrunn, Germany) and Perkadox (Dr. Grogg Chemie AG, Stetten,

Switzerland) with a ratio of 89.5:10.0:0.5. After embedding, the specimens were stored and dried at room temperature. A diamond saw (Leica 1 SP 1600, Leica Instruments GmbH, Nussloch, Germany) served for cutting circularly shaped sections of the cylindrically shaped biopsies. The sections were glued (Cementit CA 12, Merz+Benteli AG, Niederwangen, Switzerland) on opal acrylic slides (Perspex GS Acrylglas Opal 1013, Wachendorf AG, Basel, Switzerland), wrapped in aluminium foil and pressed overnight under a metal block of 1 kg weight. Further, thinning down to a thickness of $300 \mu\text{m}$ was achieved through grinding (EXACT CS400, EXACT Apparatebau, Norderstedt, Germany) and treatment with sandpaper (grit size 1200, Struers GmbH, Birmenndorf, Switzerland). Subsequently, the surfaces were polished on a Struers Planopol-V (Struers GmbH) with sandpaper (grit size 4000, Struers GmbH). The polished sections were etched with formic acid (0.7%, Sigma Aldrich) for 2 min, cleared and etched for another 2 min, rinsed with water and later surface-stained with toluidine blue (1% stock solution in 0.1 M phosphate buffer pH 8.0, Sigma Aldrich) for a duration of 10 min. The sections were digitally recorded with a microscope (Leica M420, Camera DFC 320, Leica Microsystems, Heerbrugg, Switzerland, magnification $1.0 \times 18.6 - 22.3$) using the software Image Manager 1000 (Leica Microsystems) (Stalder *et al.*, 2014). The histology images were scanned with a lateral pixel length of $1.6 \mu\text{m}$. Before applying the registration pipeline, the images were down-sampled to approximate the voxel length of the CT data. The thickness of histological sections was limited to $300 \mu\text{m}$ in the present study, because the biopsies were not de-calcified and contain the brittle grafting material. The slide, however, was only stained in the surface-near region in a thickness of approximately $10 \mu\text{m}$. Each histological slide resulted in an RGB image ranging from 300×300 to 861×861 pixels. The μCT data are 3D matrices of eight-bit gray-scale values. The data comprise a volume between $301 \times 301 \times 507$ and $301 \times 301 \times 1093$ voxels

with a binned isotropic voxel length of $8.6 \mu\text{m}$. Two datasets were recorded with a voxel length of $4.3 \mu\text{m}$ and comprise of $861 \times 861 \times 1939$ and $621 \times 621 \times 1269$ voxels, respectively. Ten datasets of nine patients were included in this study (Table 1).

The second dataset corresponds to a cylindrical specimen, obtained post-mortem from the cerebellum of a 73-year-old male. The specimen was 6 mm in diameter and 4.5 mm in length. It was extracted from the donated human brain and fixed in 4% histological-grade buffered formalin. The sample was dehydrated and paraffin-embedded according to standard pathology procedures. The cylindrical sample for the tomography measurement was extracted from the paraffin block using a metal punch with an inner diameter of 6 mm. The cerebellum specimen was scanned using the CT-system nanotom[®] m (phoenix|X-ray, GE Sensing & Inspection Technologies GmbH) in absorption contrast mode with an accelerating voltage of 60 kV and a voxel length of $3.5 \mu\text{m}$. These data were then filtered with a median filter followed by an adaptive Gaussian filter in VGStudio MAX 2.0 (Volume Graphics GmbH, Heidelberg, Germany), were resized to a voxel length of $7 \mu\text{m}$ using MATLAB[®] R2016a (The MathWorks, 135 Inc.), cropped and saved in 8 bit grayscale 3D matrix $860 \times 860 \times 901$ pixels. In total, four histological slides were sectioned (thickness $4 \mu\text{m}$) resulting in RGB images 860×860 pixels in size with a resolution of about $7 \mu\text{m}$. To obtain the histological slides, the paraffin cylinder was re-embedded in a standard paraffin block by partial melting and the addition of fresh paraffin. Sections were cut using a microtome from the upper part of the sample, left to float on a water bath and then collected one by one and mounted on glass slides by hand. The slides were then dried out and stained with haematoxylin and eosin (H&E), following a standard protocol. Images of the resulting slides were taken at $2\times$ optical magnification on a combined light microscope/digital camera system (Olympus DP73+Olympus BX43, Olympus Schweiz AG, Volketswil, Switzerland). All of the histological images were converted to grayscale, cropped and flipped, if needed.

Our approach for deformable 2D-3D registration consists of three main steps (Fig. 1). First, we find a matching slice to the histological image in the 3D μCT dataset, using our previously presented approach (Chicherova *et al.*, 2014), that matches histological slides to CT data using feature detection and matching followed by an optimal plane search based on a density-biased random sample consensus (RANSAC). Second, we rigidly register the histological image to the found slice. And lastly, starting from the initial match, we deform the plane by using an optimization framework based on NMI (see also, Table 2).

The ground truth for the counterpart of histological slide in the CT data corresponds to the registration result manually identified by four experts. The pipeline was implemented in MATLAB[®] R2016a (The MathWorks, 135 Inc.) for a Linux system running Ubuntu 15.10.

Initialization

Initialization is the first step in our method that roughly localizes the histological slide in the 3D space of the μCT data. Histological sectioning can be represented as a plane within the 3D volume of the μCT dataset, defined by the plane equation $Ax + By + Cz + D = 0$. To find the plane coefficients, we start by computing matching points between the histology image and each image of the μCT data. Corresponding points between histology images and μCT images are found with the scale and rotation invariant feature detector Speeded Up Robust Features (SURF) (Bay *et al.*, 2008). In comparison to Scale-Invariant Feature Transform (SIFT) (Lowe, 2004) and Affine SIFT (ASIFT) (Yu & Morel, 2011), it provides either more matching points or more robust correspondences (Chicherova *et al.*, 2016). The matched keypoints for each μCT image are subsequently stored in a 3D matrix. We assume that the density of the points is higher in the area which corresponds best to the histological slide. Therefore, next, we solve a density problem in 3D space, using a modified RANdom SAMple Consensus (RANSAC) algorithm (Fischler & Bolles, 1981; Chicherova *et al.*, 2014). After 15 000 iterations of the modified RANSAC, estimates of the normal vector parameters for the plane that includes the most inliers are chosen. The search parameters are constrained so that only planes within a certain tilting angle α_{jaw} , α_{cereb} are considered. For the complete pipeline and details of this method, we refer the reader to our previous work (Chicherova *et al.*, 2014). Herein, we just mention that in comparison to the previous method, we introduce an additional parameter, namely a filter radius. The specimen's background and borders often produce wrong correspondences, and so to remove them we crop the points by taking only those lying inside a circular region in the specimen (Chicherova, 2015). We calculate the filter radius as $M/2.8$, where M is the size of the square μCT image. Another modification is associated with the number of selected points for RANSAC fit P_{left} , which is calculated depending on the total number P_{total} of matching points:

$$P_{\text{left}} = \begin{cases} P_{\text{total}} & \text{if } P_{\text{total}} < 1500 \\ 1500 & \text{if } 1500 < P_{\text{total}} < 5000 \\ P_{\text{total}}/3 & \text{if } 5000 < P_{\text{total}} < 10000 \\ P_{\text{total}}/4 & \text{if } 10000 < P_{\text{total}} < 40000 \\ 10000 & \text{if } 40000 < P_{\text{total}} \end{cases} \quad (1)$$

These parameter values were selected empirically. The parameters for SURF¹ are left to default as well as for the second nearest neighbour criterion (distance ratio = 0.8). The angle between the normal to the plane and z-axis is set to $\alpha_{\text{jaw}} = \pi/8$ and $\alpha_{\text{cereb}} = \pi/36$ for the jawbone and the cerebellum datasets according to their pixel size. The proposed values of specific parameters are successfully applied to other X-ray based modalities as well (Chicherova, 2015; Chicherova

¹ [http://www.mathworks.ch/matlabcentral/fileexchange/28300-opensurfaincluding-image-warp-](http://www.mathworks.ch/matlabcentral/fileexchange/28300-opensurfaincluding-image-warp)

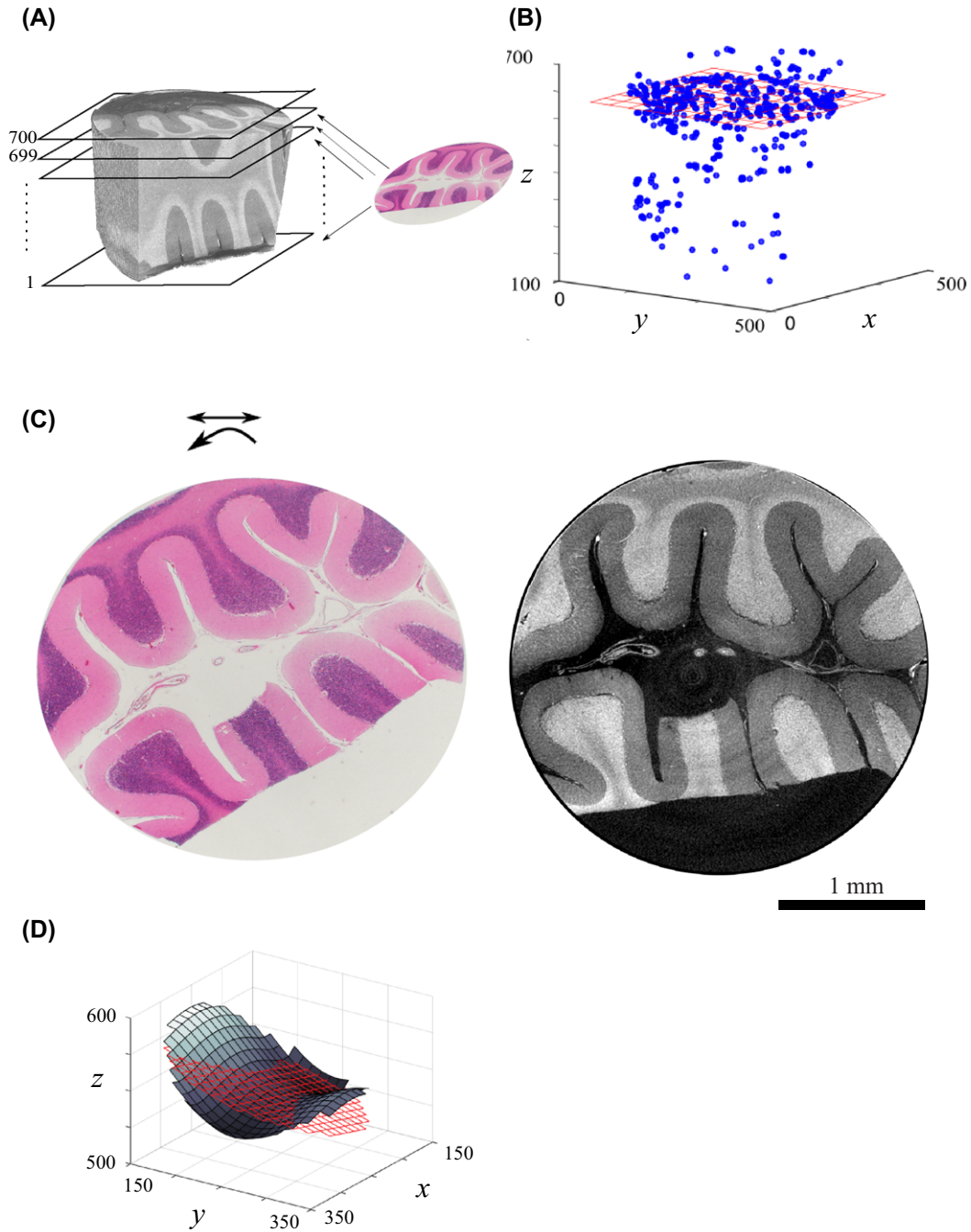


Fig. 1. Deformable 2D-3D registration pipeline. (A) Matching histology with every slice in the μ CT. (B) Plane fitting to 3D keypoints cloud. (C) Affine 2D registration of histology to the matching tomogram. (D) Deformable optimization of the found plane. The voxel positions are provided in x -, y -, and z -direction.

et al., 2016; Hieber *et al.*, 2016; Khimchenko *et al.*, 2016). Default parameters were applied for the built-in routines of RANSAC and the feature detection algorithms. The parameters, to be adjusted, are the maximal angle, the radius of the specimen, the number of iterations of RANSAC (10 000 by default) and the number of cloud points (10 000 by default). In

the computational experiments only, the maximal angle and the radius had to be adjusted to the specimen type. The radius is given by the geometry of the specimen. The maximal angle is estimated by the operator. For homogeneous specimens, such as the tissue of the cerebellum, a relatively small angle has to be selected to obtain reasonable results.

Table 2. Algorithm: deformable slide-to-volume registration.

Input: Histological image I and μ CT 3D dataset V , RANSAC default parameters (threshold = 10, # iterations 10 000, # cloud points 10'000), $\alpha_{\text{jaw}} = \pi/8$, $\alpha_{\text{cereb}} = \pi/36$
 Output: Surface coefficients c_{optim}

1. Find matching feature points between histological slide and each image in the 3D μ CT dataset
 2. Create a binary 3D matrix out of the μ CT corresponding points
 3. Assign weights to each point and filter the 3D point cloud based on weights and radius
 4. Fit a plane into the filtered 3D cloud and extract matching μ CT slice
 5. Register the histology and the μ CT image in 2D
 6. Find coefficients c_0 of the plane in Legendre bases
 7. Starting from c_0 , optimize the surface coefficients c_{optim} using NMI
- return c_{optim}
-

2D-2D registration

Having obtained the plane normal vector coordinates n_{init} from the previous step, we interpolate an image out of the μ CT dataset. In order to improve the slice position in 3D with NMI, 2D-2D registration is required. Our 2D-2D automatic registration framework is divided into two subsequent transformations, first a coarse rigid transformation and then refinement with affine registration. Let $I(x, y)$ and $J(x, y)$ be the histology image and the μ CT image obtained from the initialization. Here, $I : \Omega \subset \mathbb{R}^2 \rightarrow \mathbb{R}$ and $J : \Omega \subset \mathbb{R}^2 \rightarrow \mathbb{R}$. For coarse registration, we use a very efficient approach, called the RANSAC homography algorithm, which calculates the projective transformation matrix H between two images by using two sets of corresponding points. We use SURF to identify new corresponding points between the two images. Let $\{x_n^I, y_n^I\}$, $\{x_n^J, y_n^J\}$ be the matching points from the SURF algorithm, where $n = 1, \dots, N$ and N are numbers of putative matched points in the two images. We are looking for a linear mapping between the two sets of points that will satisfy the following equation:

$$\begin{pmatrix} x_n^J \\ y_n^J \\ 1 \end{pmatrix} = \underbrace{\begin{pmatrix} h_{1,1} & h_{1,2} & h_{1,3} \\ h_{2,1} & h_{2,2} & h_{2,3} \\ h_{3,1} & h_{3,2} & h_{3,3} \end{pmatrix}}_{:=H} \begin{pmatrix} x_n^I \\ y_n^I \\ 1 \end{pmatrix}. \quad (2)$$

The RANSAC homography algorithm solves the problem by randomly picking four corresponding point pairs and calculating the transformation matrix. Then, it counts the number of inliers, i.e. points that are mapped within a certain threshold ($t = 0.01$ voxel length), from one image to another. If the number of inliers is higher for one matrix than for the previous best one, it saves it as a possibly better homography matrix. The final matrix with the maximum number of inliers is pro-

duced after 10 000 iterations. This choice is a trade off between robustness and speed.

The main limitation of this algorithm is that it very much depends on the ratio of correctly versus wrongly matched pairs. It may produce an unrealistic transformation if the supplied points are incorrect. In some cases, the μ CT images from the initialization look quite dissimilar from the histology, which on top of the multimodal nature of the images leads to a high number of unreliable inliers. Hence, to improve the robustness of the registration, we limit the transformation to rotation and shifting, leaving only three degrees of freedom. Thus, the transformation matrix becomes for any $\alpha \in [0, 2\pi]$

$$\begin{pmatrix} x_n^J \\ y_n^J \\ 1 \end{pmatrix} = \begin{pmatrix} \cos \alpha & -\sin \alpha & t_1 \\ \sin \alpha & \cos \alpha & t_2 \\ 0 & 0 & 1 \end{pmatrix} \begin{pmatrix} x_n^I \\ y_n^I \\ 1 \end{pmatrix} = S \begin{pmatrix} x_n^I \\ y_n^I \\ 1 \end{pmatrix}. \quad (3)$$

For \vec{x} in the domain of image I , we define $I_S = I \circ S^{-1}(\vec{x}) := I(S^{-1}\vec{x})$ as an output histology image after rotation and translation. To find the new transformation matrix, we integrated the Kabsch² algorithm into the RANSAC framework. As soon as the coarse rigid registration is obtained, we improve registration with an affine transformation T . The transformation matrix T^* of the image in this case is determined by maximizing NMI between the histology image I_S and the CT image J :

$$T^* = \arg \max_T \text{NMI}[I_S \circ T^{-1}, J], \quad (4)$$

where T is a matrix in the space of all the affine transformations and NMI is calculated based on images' marginal and joint entropies E as

$$\text{NMI} = \frac{E(I_S \circ T^{-1}) + E(J)}{E(I_S \circ T^{-1}, J)}. \quad (5)$$

The final image is then calculated as $I_{AS} = I_S \circ (T^*)^{-1}$. The optimizer follows the 'one plus one' evolution strategy (Styner *et al.*, 2000). The maximum number of iterations of the optimizer is set to 300, with an initial radius of 0.004. The number of histogram bins is calculated as the median value of the Freedman–Diaconis, Scott's and Sturges' methods.

Deformable and rigid 2D-3D registration

After registering the histological image to the μ CT image in 2D, we now exploit the benefit of mutual information, which is a well-known similarity measure employed for multimodal images. NMI takes into account a dense representation of the image, whereas SURF compares only sparsely distributed points. By using every pixel intensity, more sensitive registration is achieved. In an iterative optimization framework,

² <http://ch.mathworks.com/matlabcentral/fileexchange/25746-kabsch-algorithm>

we calculate NMI between the histology and an image interpolated from a deformed surface in the μ CT volume. Surface deformations are calculated as the sum of a set of bases. With this limited set of basis functions, we approximate a function space for all possible deformations between the two modalities. As basis functions, we use associated Legendre polynomials $P_l^m(x) = (-1)^m(1-x^2)^{m/2} \frac{d^m}{dx^m} P_l(x)$ on the interval $-1 \leq x \leq 1$, where $P_l(x) = \frac{1}{2^l l!} [\frac{d^l}{dx^l} (x^2 - 1)^l]$ are nonassociated Legendre polynomials, $l \in \mathbb{Z}$ is a degree of the polynomial and $m = 0, \dots, l$ is an order of the polynomial. Legendre polynomials are solutions to the Legendre differential equation and are spherical harmonics. The choice of Legendre polynomials is based on their orthogonality, which enables linear least squares of an independent system of equations. Furthermore, they constrain surface deformations allowing for reasonable slice transformations. However, one can choose other orthogonal polynomials as bases, depending on the deformation of the specimen. Although B-splines are a commonly used basis for nonrigid deformation, this is not a reasonable solution for our case. B-spline is a piecewise deformation model for local deformations which requires control points and consequently brings a lot of degrees of freedom. This is not only computationally demanding, but it may also lead to unrealistic deformations.

We built the Legendre basis functions on a regular grid in the 3D Cartesian coordinate system. The first basis is the Legendre polynomial of zero degree ($l = 0$), $p_1 = P_0^0$, which is a plane parallel to the xy -plane. This basis accounts for shifting along the z -axis. The next two bases are Legendre polynomials of first degree ($l = 1$), $p_2 = P_1^0$, $p_3 = P_1^1$. The first order P_1^0 ($m = 0$) corresponds to an angled plane and the second order P_1^1 ($m = 1$) corresponds to a paraboloid. These bases account for angulation of the plane and parabolic deformation of the tissue. We enrich our bases with $p_4 = P_2^0$, $p_5 = P_2^2$, $p_6 = P_4^0$, $p_7 = P_4^1$, $p_8 = P_5^1$ Legendre polynomials. In total, we obtain 15 bases $P = \bigcup_{k=1}^{15} p_k$, including the transposed ones of each basis except the first one. The initial search starts from the plane obtained from the initialization step. We represent this plane with our base functions and extract associated coefficients. Let $F = f(x, y)$ be the plane obtained from fitting RANSAC to the matching points. To represent this function with Legendre polynomials, we sample randomly M times this plane $F_1 = f(x_1, y_1), \dots, F_M = f(x_M, y_M)$ and obtain a vector $\psi = [F_1, \dots, F_M]^T \in \mathbb{R}$ of z coordinates that lie on this plane. The same x, y coordinates of the sample points are then used to select z -values of the Legendre basis functions. Thus, for each basis, we obtain a vector $\hat{p}_k = [p_k(x_1, y_1) \dots p_k(x_M, y_M)]^T$. Therefore, the plane can be represented in Legendre bases as $\psi = \sum_{k=1}^{15} c_k \hat{p}_k$, where $c_k \in \mathbb{R}$ are the basis coefficients.

We calculate the coefficients as a least square solution of a system of linear equations. These coefficients are then provided as arguments in an optimization framework which maximizes NMI.

Table 3. Median errors for the rigid NMI-based registration.

Dataset #	1	2	3	4	5	6	7	8
Tilting angle error [deg]	1.4	0.6	0.9	0.3	0.8	1.9	0.7	0.6
Distance error [μm]	36	7	12	2	8	34	8	8

$$c_{\text{optim}} = \arg \max_c \text{NMI}[J(c), I_{AS}], \quad (6)$$

where $J(c)$ is an interpolated image from a surface obtained with \hat{p}_k basis functions. As an optimization algorithm, we use a bounded version of the Nelder–Mead simplex direct search³, which is one of the best solutions for non-smooth objective functions (Maes *et al.*, 1999; Wachowiak *et al.*, 2004). The Nelder–Mead simplex is a local optimizer that provides accurate results when the initial orientation is close to the true transformation. To increase the search space, we initialize the optimization with 20 random planes close to the initialization plane. After 20 iterations, we choose the one with the highest NMI.

In this work, we explore both rigid and nonlinear deformation models. The difference between them is the number of bases in the optimization. For rigid 2D-3D registration, we take only the three Cartesian bases x, y, z . Therefore, the rigid pipeline optimizes the normal vector coordinates to the plane $\vec{n} = [A \ B \ C]^T$. For nonlinearly deformable surfaces, we use the Legendre polynomials. The following constraints are used in both frameworks. The plane angle is set to α_{jaw} and α_{cereb} for the corresponding data, and the shift along the vertical axis is ± 80 slices. The brute force constraints lie in the same interval. We also limit the Legendre bases to exploit only feasible deformations $[10^4, 10^4, 10^4, 5 \cdot 10^3, 10^2, 10^2]$ for the p_3 until p_8 correspondingly.

Results

Jaw bone dataset - the rigid registration framework

The rigid NMI-based registration framework was evaluated on jaw bone datasets. The histological slides in these datasets contained only limited nonrigid deformations perpendicular to the cutting plane, due to the presence of hard, bony tissue. Therefore, for these datasets, it was sufficient to perform rigid registration. To assess the performance of the framework quantitatively, we calculated the angle between the normal vector obtained with optimization and the manually found example (Table 3), which gave us an idea of how well the tilting of the plane had been determined with the method. We also computed the distance between the two planes to determine how far the found plane was from the ground truth. We calculated the distances from the origin along the z -axis for the optimized plane and the ground truth, and then we subtracted them

³ <http://ch.mathworks.com/matlabcentral/fileexchange/8277-fminsearchbnd-fminsearchcon>

from each other. The median values of these errors for eight datasets are summarized in Table 3. Manual registrations were subsequently improved by four experts, which is regarded as the ground truth in this study. In addition, to evaluate the variability of the ground truth, we calculated mean standard variation of further manual registration values for four histological slides. Deviation of vertical position was seven slices and of the tilting angle was 2° . As the high-resolution CT data exhibit many anatomical details, the manual results were very similar to histological images (see Khimchenko (2016)).

The method accurately determined the tilting angle of the plane. Indeed, the angle error did not exceed 1.4° . The median distance error for the optimized rigid registration was also very low for most of the datasets. The largest errors were in the first and sixth datasets, 36 and $34\ \mu\text{m}$, respectively. From a visual assessment, we consider a distance error of $60\ \mu\text{m}$ as a reasonable registration. This length corresponds to the size of the characteristic anatomical structures of the human jaw, i.e. the Haversian canals with a diameter of about $60\ \mu\text{m}$. Therefore, according to this assessment, our algorithm registered well 47 out of 58 histological slides. The time needed for the linear interpolation of a 2D image from a 3D volume grows as $O(N)$, where N is the number of voxels in the 3D datasets. We compared the computational effort of two datasets from the same patient E, where two pieces of the biopsy were processed separately. The average computational time for registering one histological slide in a volume of $621 \times 621 \times 1269$ voxels was 26.2 min (3.6 min for SURF) compared to 2.8 min (0.3 min for SURF) in a $301 \times 301 \times 507$ voxel dataset. Consequently, a 10 times larger volume gives rise to an increase of the computational effort by a factor of approximately nine. All the calculations were performed sequentially in MATLAB[®] R2016a on Ubuntu 15.10 with 64 GB of RAM and Intel[®] Xeon E5-2620 v3 (6 cores, 2.4 GHz/3.2 GHz Turbo).

To determine if the new pipeline had improved the initial matching, we compared the SURF-based and the rigid NMI-based pipelines with the ground truth. We calculated the tilting error and the distance error for both methods (Fig. 2).

From the comparative distance errors, one can see that in the majority of the cases, slice localization improved. Furthermore, the dispersion of the results decreased, which suggests a more stable behaviour. However, for the first dataset, there is a small deterioration. This dataset had a very high resolution, so there were several reasonable registration positions. Hence, for most of the histologies, the difference in registration between the two methods was not significant. The largest improvement was achieved in dataset #7, e.g. the distance error dropped from 251 to $0\ \mu\text{m}$. The method shows a general improvement for the tilting angle. The median error for the tilting angle does decrease, but there are outliers in some of the datasets. This is due to poor 2D-2D registration when the found initialization slice was far from the ground truth. Two examples of histological sections along with the registration results from both methods are shown in Figure 3. The

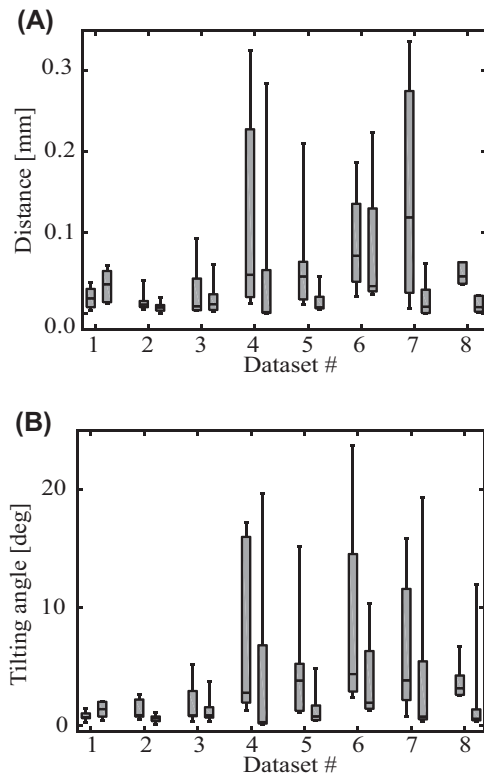


Fig. 2. Comparative error for the position (A) and the angle (B) of the plane for eight jawbone datasets. On the x-axis are shown the performance of the SURF- (left) and NMI (right)-based methods for each dataset. The median values are shown as black horizontal lines inside the boxes, 25th and 75th percentiles as bottom and top lines of the box, minimum and maximum values as bottom and top whiskers.

first method found a relevant match for the histology, but there are numerous local dissimilarities between the images. The nonparametric significance test shows that the pipeline with optimization improves registration (Kruskal–Wallis test p -value = 0.0013).

In datasets #9 and #10, the proposed method with the default setup failed to find a reasonable registration for the majority of the slides due to a large tilting angle of approximately 20° combined with an additional issue. For dataset #9, the registration was successful after having adjusted the contrast of the individual histological slides or a rotation of the CT data to match the histological cutting direction (Stalder *et al.*, 2014). The broken specimen of dataset #10 showed an incomplete cylindrical shape and required a rotation of the CT data or an adaptation of the filter radius for a successful registration. The illumination invariance of the SURF descriptor could not account for a 100 gray value difference. Furthermore, in one of these datasets, on top of the high tilting angle (22°), X-ray absorption values differed for the same tissue in the bottom of the specimen and on the top. This is why it was especially challenging to register this dataset and the

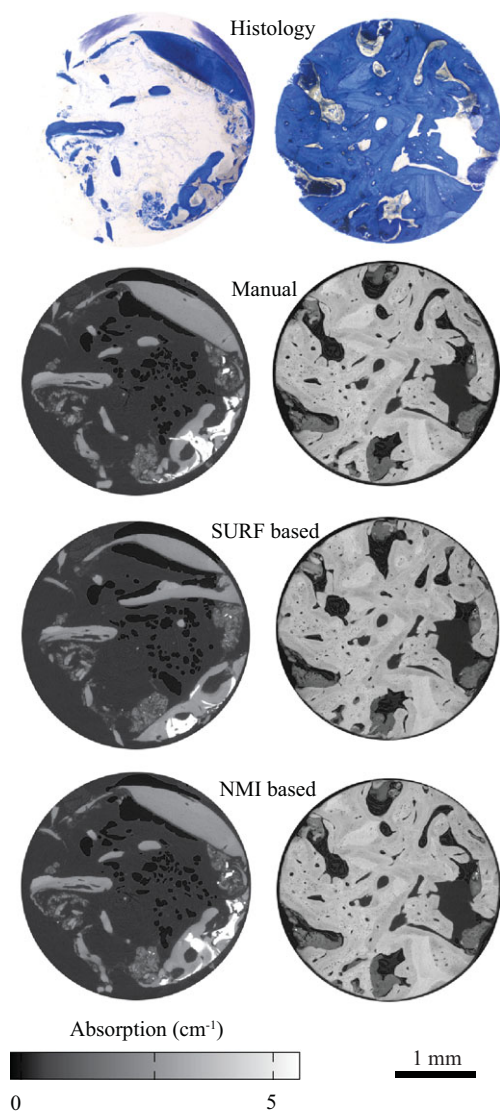


Fig. 3. Comparative slide registration for the datasets #4 (right) and #7 (left).

approach found only one reasonable registration out of four. In the dataset #2, however, the algorithm localized two histological images which were only one slice away from the ground truth. Also, the distance error for one histological slide in the dataset #8 would not fit into the boxplot region, and so it was removed for better visualization.

Jaw bone dataset - the deformable registration framework using simulations

Additionally, we evaluated the deformable registration framework on the jawbone datasets, using simulation. We created artificial histological slides by simulating deformed surfaces in 3D space. With these surfaces, we extracted an image from the μ CT volume, following which we used this image as an

artificial histology section and ran it through the entire NMI-based deformable pipeline. An example of the surface and the resulting fit of the deformable pipeline for two artificial histologies is shown in Figure 4. With a color bar, we show the distance difference between the found surface and the artificial ground truth. In total, we evaluated five histological slides, and on average it took 58 min per slide. The maximum difference in the region of interest did not exceed $50 \mu\text{m}$.

Cerebellum datasets - the deformable registration framework

In contrast to the bone data, the cerebellum specimen included large non-linear deformations (Hieber *et al.*, 2016; Khimchenko *et al.*, 2016). Hence, we evaluated the deformable registration framework on this dataset. In total, four histological sections were available. The average computation time for one slide grew to 6.8 h, owing to the effort in optimization that is required to determine the deformations. In addition, the homogeneity of the tissue requires a larger number of optimization steps. For a quantitative assessment, we compared distances from the found surface to the manually found landmarks (Fig. 5). Manual registration was based on point-to-point correspondence of characteristic features such as vessels, cell groups and cracks. Then, a polynomial surface using the Matlab Curve Fitting Toolbox was fitted into the points. In three out of four histological slides, there was an improvement in registration. The median distance error improved by $33 \mu\text{m}$ for all slides. For the histology #2, registration did not improve as the result of an image artefact. The histological section was cut from the top part of the specimen, where the tomography slices were distorted and part of the volume was removed.

Figure 6 shows an example of the first histological image and corresponding slices found with both approaches. The SURF-based method found a slice which was 0.8 mm away from the manual surface for more than half of the histology. Moreover, the deformable fit improved registration by reducing the area of high distance difference. Even though the median distance from the manual landmarks increased by $21.6 \mu\text{m}$, the overall registration of this histological slide improved, due to the decreased dispersion of the distances.

Discussion

The proposed algorithm is a coarse-to-fine registration technique that starts with the localization of a sectioning plane and finishes with the complete registration of 2D histology into the 3D space. Although hard X-ray tomography provides the 3D spatial distribution of the X-ray attenuation coefficients, the histology images exhibit the 2D spatial distribution of the stain intensity integrated perpendicular to the slide. Therefore, the contrast mechanisms are complementary. In order to exclude the impact of the contrast mechanisms, intentionally distorted CT slices were registered to the measured 3D CT data. This approach permits the error estimation excluding the impact of

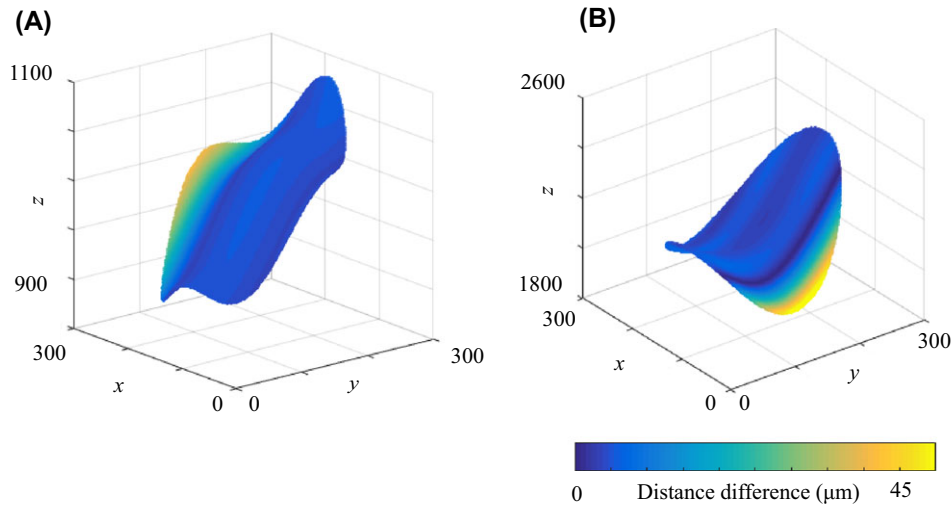


Fig. 4. Optimized fitting surfaces for the simulated histological slides colored according to the distance error from the ground truth. The voxel positions are provided in x -, y -, and z -direction.

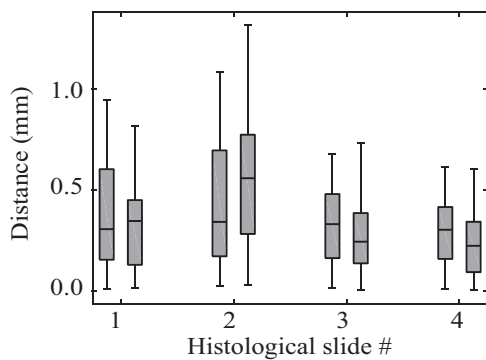


Fig. 5. Comparative distance error to the manual landmarks for four histological sections in the cerebellum dataset. On the x -axis are shown the performance of the SURF- (left) and NMI- (right) based methods for each section. The median values are shown as black horizontal lines inside the boxes, 25th and 75th percentiles as bottom and top lines of the box, minimum and maximum values as bottom and top whiskers.

the contrast mechanism and precise error can be evaluated because the ground truth is predefined. The application of the proposed method is not limited to histology to μ CT registration – it can be applied easily to any slide-to-volume registration (Markelj *et al.*, 2012). For example, another interesting potential application is registering 2D histology to 3D MRI data (Dauguet *et al.*, 2007; Liu *et al.*, 2012; Goubran *et al.*, 2015). The important feature of our approach is that in contrast to other methods, it does not require any segmentation or other data-dependent preprocessing for images of the same size.

Overall, the method showed high accuracy in slice localization. Indeed, it allocated 47 out of 58 histological slides with high precision (distance error < 62 μ m). Furthermore, after visual inspection, we identified that eight more slices were in fact close to the ground truth position (distance

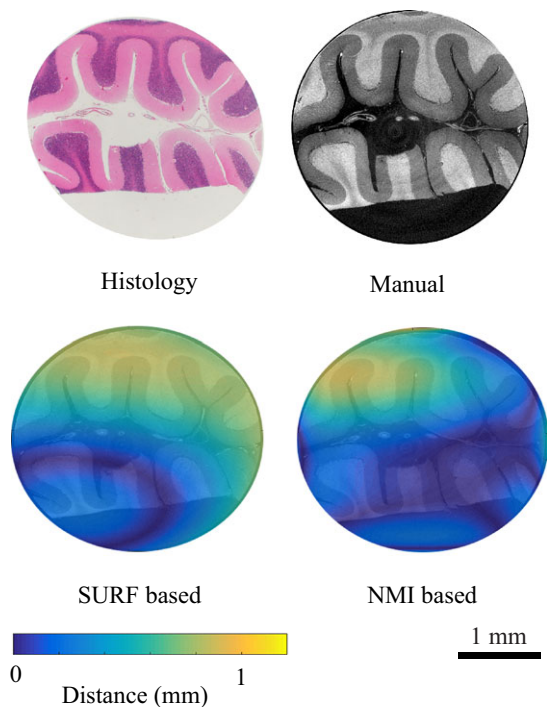


Fig. 6. Comparative slide registration for the first slide colored according to the distance error from the ground truth.

error < 1 mm). The median registration error for the 10 jaw bone volumes of 8.4 μ m is well below the slide thickness of 300 μ m and below the near-surface region that contributes to the stain intensity of the histology slide. Hence, one can conclude that the proposed procedure provides a sound registration result. The identification of the correct cutting angle correlates with the correct localization of the slide; indeed, the

improvement in the tilting angle shows a pattern similar to the distance error improvement (Fig. 2), whereas deformable registration shows high accuracy in simulations, even for highly deformed artificial slices. The distance from the ground truth surface was less than 20 μm for the majority of the slices.

The initialization provides a plane in the 3D dataset where the most matching points are found. To accelerate the later optimization based on NMI, the histology slide should be registered rigidly to the obtained CT slice. Unfortunately, as this step relies on feature correspondences and the heuristic transformation matrix calculation, the resulting 2D-2D registration can vary for different iterations. The solution to this problem is either visual inspection or parameter optimization. However, in the majority of cases, the result of initialization is of sufficient quality and the algorithm does not need any intervention. Additional improvements to this step could be achieved with one of the multimodal histology 2D-2D registration algorithms (Jacobs *et al.*, 1999; du Bois d'Aische *et al.*, 2005; Li *et al.*, 2006; Pitiot *et al.*, 2006; Hallack *et al.*, 2015).

Another limitation of our method is that it uses the SURF algorithm for feature detection. This descriptor is built using the neighbourhood gradient around the keypoint. Hence, low-contrast images or images of mostly homogeneous tissue are likely to produce a lot of false matching points, which in turn hampers registration. One potential solution is to use another feature detector (Self-Similarity (Shechtman & Irani, 2007), ORB (Rublee *et al.*, 2011), etc.) or image preprocessing, for example, by attenuating the illumination difference between grayscale histology and μCT images.

Furthermore, output-matching slices after the SURF-based method can vary somewhat, depending on the parameters – sensitive parameters are the filter radius and the plane angulation constraints. For example, in dataset #4, the registration could not be achieved without radial filtering of the point cloud. With adjusted values, however, we were able to register all of the histological slides accurately.

The computation time of the algorithm is dominated by the optimization part of the method. Therefore, the method could benefit from faster 3D pixel interpolation approaches. Another possible improvement to 2D-3D optimization could be achieved by using a global optimizer such as swarm (Wachowiak *et al.*, 2004), which would make the time-consuming brute-force search unnecessary or by patch-wise registration (Ferrante & Paragios, 2013). Computational speed-up can be also attained by implementing the pipeline in C++, using parallel programming.

In conclusion, we have proposed a fully automatic approach for multi-modal 2D-3D registration which combines feature- and intensity-based approaches to accurately register a 2D slice to volume data. We have also demonstrated the high accuracy and reliability of the method and outlined potential applications beyond the particular histology- μCT registration analyzed herein.

Acknowledgements

The authors are very grateful to Anja Stalder and Marcel Würsch for the manual ground truth data. The authors thank Bernd Ilgenstein for the jaw biopsies and Stefan Stübinger for their histological sectioning as well as J. Hench and G. Schweighauser of the Neuropathology Department of the Basel University Hospital for providing the cerebellum sample and helping with the special preparation required for tomography measurement. Moreover, they thank the staff of the synchrotron facilities and Hans Deyhle as well as Georg Schulz for data treatment. Beamtime was granted through the project proposals I-20110780 EC and I-20110780 EC (HASYLAB at DESY, Hamburg, Germany). The work was funded by the Swiss National Science Foundation (SNSF) project 150164. Data were obtained with the support of SNSF projects 147172 and 133802.

References

- Alic, L., Haeck, J.C., Bol, K. *et al.* (2011) Facilitating tumor functional assessment by spatially relating 3D tumor histology and *in vivo* MRI: image registration approach. *PLoS One* 6(8), e22835.
- Arganda-Carreras, I., Fernández-González, R., Muñoz-Barrutia, A. & Ortiz-De-Solorzano, C. (2010) 3D reconstruction of histological sections: application to mammary gland tissue. *Microsc. Res. Tech.* 73(11), 1019–1029.
- Bardinet, E., Ourselin, S., Dormont, D., Malandain, G., Tandé, D., Parain, K., Ayache, N. & Yelnik, J. (2002) Co-registration of histological, optical and MR data of the human brain. *In Lecture Notes in Computer Science - MICCAI 2002*, vol. 2488, pp. 548–555.
- Bay, H., Ess, A., Tuytelaars, T. & Van Gool, L. (2008) Speeded-up robust features (SURF). *Comp. Vis. Image Understand.* 110, 346–359.
- Bernhardt, R., Scharnweber, D., Müller, B., Thurner, P., Schliephake, H., Wyss, P., Beckmann, F. & Goebbels, J. (2004) Comparison of microfocus- and synchrotron X-ray tomography for the analysis of osteointegration around Ti6Al4V implants. *Eur. Cells Mater.* 7, 42–51.
- Breen, M.S., Lazebnik, R.S. & Wilson, D.L. (2005) Three-dimensional registration of magnetic resonance image data to histological sections with model-based evaluation. *Ann. Biomed. Eng.* 33(8), 1100–1112.
- Ceritoglu, C., Wang, L., Seimon, L.D., Csernansky, J.G., Miller, M.I. & Ratanathaner, J.T. (2010) Large deformation diffeomorphic metric mapping registration of reconstructed 3D histological section images and *in vivo* MR images. *Front. Hum. Neurosci.* 4, 1–11.
- Chicherova, N., Cattin, P., Schulz, G., Fundana, K., Müller, B. & Hieber, S.E. (2015) Automatic matching of grating-based phase tomography dataset with histology. *Eur. Cells Mater.* 30(Suppl. 1), 34.
- Chicherova, N., Fundana, K., Müller, B. & Cattin, P.C. (2014) Histology to μCT data matching using landmarks and a density biased RANSAC. *In Lecture Notes in Computer Science - MICCAI 2014*, vol. 8673, pp. 243–250.
- Chicherova, N., Hieber, S.E., Schulz, G., Khimchenko, A., Bikis, C., Cattin, P.C. & Müller, B. (2016) Automatic histology registration in application to X-ray modalities. *Proc. SPIE* 9967, 996708.
- Dauguet, J., Delzescaux, T., Condé, F., Mangin, J.-F., Ayache, N., Hantraye, P. & Frouin, V. (2007) Three-dimensional reconstruction of stained

- histological slices and 3D non-linear registration with *in-vivo* MRI for whole baboon brain. *J. Neurosci. Methods* **164**(1), 191–204.
- du Bois d'Aische, A., De Craene, M., Geets, X., Gregoire, V., Macq, B. & Warfield, S.K. (2005) Efficient multi-modal dense field non-rigid registration: alignment of histological and section images. *Med. Image Anal.* **9**(6), 538–546.
- Ferrante, E. & Paragios, N. (2013) Non-rigid 2D-3D medical image registration using Markov random fields. In *Lecture Notes in Computer Science - MICCAI 2013*, vol. 8151, pp. 163–170.
- Ferrante, E. & Paragios, N. (2017) Slice-to-volume medical image registration: a survey. *Med. Image Anal.* **39**, 101–123.
- Fischler, M.A. & Bolles, R.C. (1981) Random sample consensus: a paradigm for model fitting with applications to image analysis and automated cartography. *Commun. ACM* **24**, 381–395.
- Germann, M., Morel, A., Beckmann, F., Andronache, A., Jeanmond, D. & Müller, B. (2008) Strain fields in histological slices of brain tissue determined by synchrotron radiation-based micro computed tomography. *J. Neurosci. Methods* **170**, 149–155.
- Goubran, M., Crukley, C., de Ribaupierre, S., Peters, T.M. & Khan, A.R. (2013) Image registration of *ex-vivo* MRI to sparsely sectioned histology of hippocampal and neocortical temporal lobe specimens. *Neuroimage* **83**, 770–781.
- Goubran, M., de Ribaupierre, S., Hammond, R.R., Currie, C., Burneo, J.G., Parrent, A.G., Peters, T.M. & Khan, A.R. (2015) Registration of *in-vivo* to *ex-vivo* MRI of surgically resected specimens: a pipeline for histology to *in-vivo* registration. *J. Neurosci. Methods* **241**, 53–65.
- Hallack, A., Papiéz, B.W., Wilson, J., Wang, L.M., Maughan, T., Gooding, M.J. & Schnabel, J.A. (2015) Correlating tumour histology and *ex vivo* MRI using dense modality-independent patch-based descriptors. In *Lecture Notes in Computer Science*, vol. 9467, pp. 137–145.
- Hieber, S.E., Bikis, C., Khimchenko, A., Schweighauser, G., Chicherova, N., Schulz, G. & Müller, B. (2016) Tomographic brain imaging with nucleolar detail and automatic cell counting. *Sci. Rep.* **6**, 32156–32167.
- Hoerth, R.M., Baum, D., Knötzel, D. *et al.* (2015) Registering 2D and 3D imaging data of bone during healing. *Connect. Tissue Res.* **56**(2), 133–143.
- Humm, J., Ballon, D., Hu, Y. *et al.* (2003) A stereotactic method for the three-dimensional registration of multi-modality biologic images in animals: NMR, PET, histology, and autoradiography. *Med. Phys.* **30**(9), 2303–2314.
- Jacobs, M.A., Windham, J.P., Soltanian-Zadeh, H., Peck, D.J. & Knight, R.A. (1999) Registration and warping of magnetic resonance images to histological sections. *Med. Phys.* **26**(8), 1568–1578.
- Khimchenko, A. (2016) Manual landmarks selection in the cerebellum dataset [last visited January 2, 2018]. URL: <https://www.youtube.com/watch?v=TwfeiXfgZDM>.
- Khimchenko, A., Deyhle, H., Schulz, G. *et al.* (2016) Extending two-dimensional histology into the third dimension through conventional micro computed tomography. *Neuroimage* **139**, 26–36.
- Kim, B., Boes, J.L., Frey, K.A. & Meyer, C.R. (1997) Mutual information for automated unwarping of rat brain autoradiographs. *Neuroimage* **5**(1), 31–40.
- Kim, T.-S., Singh, M., Sungkara, W., Zarow, C. & Chui, H. (2000) Automatic registration of postmortem brain slices to MRI reference volume. *IEEE Trans. Nucl. Sci.* **47**(4), 1607–1613.
- Krauth, A., Blanc, R., Poveda, A., Jeanmonod, D., Morel, A. & Székely, G. (2010) A mean three-dimensional atlas of the human thalamus: generation from multiple histological data. *Neuroimage* **49**(3), 2053–2062.
- Lazebnik, R.S., Lancaster, T.L., Breen, M.S., Lewin, J.S. & Wilson, D.L. (2003) Volume registration using needle paths and point landmarks for evaluation of interventional MRI treatments. *IEEE Trans. Med. Imag.* **22**(5), 653–660.
- Li, G., Nikolova, S. & Bartha, R. (2006) Registration of *in vivo* magnetic resonance T1-weighted brain images to triphenyltetrazolium chloride stained sections in small animals. *J. Neurosci. Methods* **156**(1), 368–375.
- Liu, Y., Sajja, B.R., Uberti, M.G., Gendelman, H.E., Kielian, T. & Boska, M.D. (2012) Landmark optimization using local curvature for point-based nonlinear rodent brain image registration. *J. Biomed. Imaging* **2012**, 1.
- Lowe, D.G. (2004) Distinctive image features from scale-invariant keypoints. *Int. J. Comp. Vis.* **60**, 91–110.
- Lundin, E.L., Stauber, M., Papageorgiou, P., Ehrbar, M., Ghayor, C., Weber, F.E., Tanner, C. & Goksel, O. (2017) Automatic registration of 2D histological sections to 3D microCT volumes: trabecular bone. *Bone* **105**, 173–183.
- Maes, F., Vandermeulen, D. & Suetens, P. (1999) Comparative evaluation of multiresolution optimization strategies for multimodality image registration by maximization of mutual information. *Med. Image Anal.* **3**(4), 373–386.
- Markelj, P., Tomaževič, D., Likar, B. & Pernuš, F. (2012) A review of 3D/2D registration methods for image-guided interventions. *Med. Image Anal.* **16**(3), 642–661.
- Meyer, C.R., Moffat, B.A., Kuszpit, K., Bland, P.L., Chenevert, T., Rehemtulla, A. & Ross, B. (2006) A methodology for registration of a histological slide and *in vivo* MRI volume based on optimizing mutual information. *Mol. Imaging* **5**(1), 16–23.
- Mosaliganti, K., Pan, T., Sharp, R. *et al.* (2006) Registration and 3D visualization of large microscopy images. *Proc. SPIE* **6144**, 61442V.
- Müller, B., Deyhle, H., Lang, S., Schulz, G., Bormann, T., Fierz, F.C. & Hieber, S.E. (2012) Three-dimensional registration of tomography data for quantification in biomaterials science. *Int. J. Mater. Res.* **103**(2), 242–249.
- Nir, G. & Salcudean, S.E. (2013) Registration of whole-mount histology and tomography of the prostate using particle filtering. *Proc. SPIE* **8676**, 86760E.
- Osechinskiy, S. & Kruggel, F. (2010) Slice-to-volume nonrigid registration of histological sections to MR images of the human brain. *Anat. Res. Int.* **287860**, 1–7.
- Ou, Y., Shen, D., Feldman, M., Tomaszewski, J. & Davatzikos, C. (2009) Non-rigid registration between histological and MR images of the prostate: a joint segmentation and registration framework. In *IEEE Computer Vision and Pattern Recognition Workshops*, pp. 125–132.
- Ourselin, S., Bardenet, E., Dormont, D. *et al.* (2001) Fusion of histological sections and MR images: towards the construction of an atlas of the human basal ganglia. In *Lecture Notes of Computer Science - MICCAI 2001*, vol. 2208, pp. 743–751.
- Pardasani, U., Baxter, J.S., Peters, T.M. & Khan, A.R. (2016) Single slice US-MRI registration for neurosurgical MRI-guided US. *Proc. SPIE* **9786**, 97862D.
- Park, H., Piert, M.R., Khan, A., Shah, R., Hussain, H., Siddiqui, J., Chenevert, T.L. & Meyer, C.R. (2008) Registration methodology for histological sections and *in vivo* imaging of human prostate. *Acad. Radiol.* **15**(8), 1027–1039.
- Particelli, F., Mecozzi, L., Beraudi, A., Montesi, M., Baruffaldi, F. & Viceconti, M. (2012) A comparison between micro-CT and histology for the evaluation of cortical bone: effect of polymethylmethacrylate embedding on structural parameters. *J. Microsc.* **245**(3), 302–310.

- Pitiot, A., Bardinet, E., Thompson, P.M. & Malandain, G. (2006) Piecewise affine registration of biological images for volume reconstruction. *Med. Image Anal.* **10**, 465–483.
- Pluim, J.P., Maintz, J.A., Viergever, M. *et al.* (2003) Mutual-information-based registration of medical images: a survey. *IEEE Trans. Med. Imaging* **22**(8), 986–1004.
- Ruble, E., Rabaud, V., Konolige, K. & Bradski, G. (2011) ORB: an efficient alternative to SIFT or SURF. In *IEEE International Conference on Computer Vision (ICCV 2011)*, pp. 2564–2571.
- Sarve, H., Lindblad, J. & Johansson, C.B. (2008) Registration of 2D histological images of bone implants with 3D SR μ CT volumes. *Adv. Vis. Comput.* **5358**, 1071–1080.
- Schormann, T., Dabringhaus, A. & Zilles, K. (1995) Statistics of deformations in histology and application to improved alignment with MRI. *IEEE Trans. Med. Imaging* **14**(1), 25–35.
- Schormann, T. & Zilles, K. (1998) Three-dimensional linear and nonlinear transformations: an integration of light microscopical and MRI data. *Hum. Brain Mapp.* **6**(5–6), 339–347.
- Schulz, G., Crooijmans, H., Germann, M., Scheffler, K., Müller-Gerbl, M., Bikis, C. & Müller, B. (2011) Three-dimensional strain fields in human brain resulting from formalin fixation. *J. Neurosci. Methods* **202**, 17–27.
- Schulz, G., Waschkies, C., Pfeiffer, F., Zanette, I., Weitkamp, T., David, C. & Müller, B. (2012) Multimodal imaging of human cerebellum—merging X-ray phase microtomography, magnetic resonance microscopy and histology. *Sci. Rep.* **2**, 826–833.
- Seise, M., Alhonnoro, T., Kolesnik, M. *et al.* (2011) Interactive registration of 2D histology and 3D CT data for assessment of radiofrequency ablation treatment. *J. Pathol. Inform.* **2**(2), 9.
- Shechtman, E. & Irani, M. (2007) Matching local self-similarities across images and videos. In *IEEE Conference on Computer Vision and Pattern Recognition (CVPR 2007)*, pp. 18–23.
- Stalder, A.K., Ilgenstein, B., Chicherova, N., Deyhle, H., Beckmann, F., Müller, B. & Hieber, S.E. (2014) Combined use of micro computed tomography and histology to evaluate the regenerative capacity of bone grafting materials. *Int. J. Mater. Res.* **105**(7), 679–691.
- Studholme, C., Hill, D.L. & Hawkes, D.J. (1999) An overlap invariant entropy measure of 3D medical image alignment. *Pattern Recognit.* **32**(1), 71–86.
- Styner, M., Brechbühler, C., Székely, G. & Gerig, G. (2000) Parametric estimate of intensity inhomogeneities applied to MRI. *IEEE Trans. Med. Imaging* **19**(3), 153–165.
- Taylor, L.S., Porter, B.C., Nadasdy, G. *et al.* (2004) Three-dimensional registration of prostate images from histology and ultrasound. *Ultrasound Med. Biol.* **30**(2), 161–168.
- Thurner, P., Beckmann, F. & Müller, B. (2004) An optimization procedure for spatial and density resolution in hard X-ray micro computed tomography. *Nucl. Instr. Meth. Phys. Res. B* **225**, 599–603.
- Tsai, C.-L., Lister, J., Björnsson, C., Smith, K., Shain, W., Barnes, S.C. & Roysam, B. (2011) Robust, globally consistent and fully automatic multi-image registration and montage synthesis for 3-D multi-channel images. *J. Microsc.* **243**(2), 154–171.
- Tsai, C.-L., Warger II, W., Laevsky, G. & Dimarzio, C. (2008) Alignment with sub-pixel accuracy for images of multi-modality microscopes using automatic calibration. *J. Microsc.* **232**(1), 164–176.
- Viola, P. & Wells III, W.M. (1997) Alignment by maximization of mutual information. *Int. J. Comp. Vis.* **24**(2), 137–154.
- Wachowiak, M.P., Smolíková, R., Zheng, Y., Zurada, J.M. & Elmaghraby, A.S. (2004) An approach to multimodal biomedical image registration utilizing particle swarm optimization. *IEEE Trans. Evol. Comput.* **8**(3), 289–301.
- Yu, G. & Morel, J. (2011) ASIFT: an algorithm for fully affine invariant comparison. *Image Process. On Line* **1**, 11–38.
- Zhan, Y., Ou, Y., Feldman, M., Tomaszewski, J., Davatzikos, C. & Shen, D. (2007) Registering histologic and MR images of prostate for image-based cancer detection. *Acad. Radiol.* **14**(11), 1367–1381.